Numerical simulation of galvanic corrosion by boundary node method

†*Sanshan Tu, Hongqi Yang, Liang Zhou, and Yi Huang

School of Naval Architecture, Dalian University of Technology, Dalian, China.

*Presenting author: tss71618@163.com
†Corresponding author: tss71618@163.com

Abstract

The electric potential in the electrolyte obeys Laplace equation in galvanic corrosion problems. In this research, we developed the moving Kriging interpolation based boundary node method (MKIBNM) for galvanic corrosion problems to predict the corrosion rate and track the moving boundary of the corroding constituent. The numerical results obtained from MKIBNM are compared with the experimental results.

Keywords: Laplace equation; Galvanic corrosion; Moving Kriging interpolation; Boundary node method;

1 Introduction

The conventional methods such as finite element method (FEM) and boundary element method (BEM) require elements to construct the shape function, while a meshless method constructs the shape function entirely based on scattered nodes with greater flexibility and higher precision.

The meshless methods have been used in many engineering problems such as fluid mechanics problems [1], solid mechanics problems [2] [3], Elasticity Problems [4] [15], viscoelasticity problems [5], heat conduction problems [6] [20] and elastodynamic problems [14] [16].

Boundary integral equation (BIE) based meshless methods are an important part of meshless methods. The boundary node method (BNM) is firstly proposed by Mukherjee et al. [7]-[10] based on the moving least square (MLS) method [11] and BIE. Unlike many other 'domain' type meshless methods, the BNM only requires scattered nodes on the 1-D bounding curve of a 2-D area or the 2-D bounding surface of a 3D body and a simple boundary cell structure for numerical integration. The idea of BNM has been developed by many other researchers such as Zhu et al. [12] [13], Liew et al.[14]-[16], Ren et al. [17] [18] and Li et al. [19] with different approximating methods.

Approximating methods play an important role in meshless methods. The moving Kriging interpolation (MKI) method [20], also known as the radial point interpolation method (RPIM) [2], is an important approximating method to construct shape functions in meshless methods. MKI has partition of unity property, consistency property and high approximation precision. Besides, the shape functions constructed by MKI possess Kronecker delta property. Then, the essential boundary condition can be imposed directly and easily. Li et al. [19] have proposed the moving Kriging interpolation-based boundary node method (MKIBNM) by combing moving Kriging interpolation (MKI) with BIE for potential problems. MKIBNM has a high precision and can directly impose boundary conditions. Therefore, we chose MKIBNM to simulate galvanic corrosion.

Galvanic corrosion is an example of a process undergoing electro dissolution that aggravates metal corrosion and limits the widespread use of alloys such as the use of magnesium alloys in the automotive industry. Researchers have investigated galvanic corrosions by both experiments and numerical simulations [21]-[25]. We, for the first time, developed the MKIBNM method to investigate the corrosion behavior of galvanic couples. MKIBNM can easily track the moving boundary of the moving boundary of the corroding constituent

without re-meshing. We use the case and experimental results from reference [21] [22] to demonstrate the accuracy and flexibility of BNM.

2 Moving kriging interpolation (MKI) on 2D boundary

In 2D boundary meshless methods, we use one parametric coordinate s to approximate boundary function values. The shape function $\boldsymbol{N}(s)$ in MKI is defined by

$$\boldsymbol{N}(s) = \boldsymbol{p}(s)\boldsymbol{A} + \boldsymbol{r}^T(s)\boldsymbol{B} \tag{1}$$

where $\boldsymbol{p}(s) = [p_1(s), p_2(s), \text{L}, p_m(s)]$, $p_j(s) = s^{j-1}$ $(j = 1, 2, \text{L}, m)$ are monomial basis functions, m is the number of terms of basis. $\boldsymbol{r}(s)$ is the $n \times 1$ vector of correlation between point at s and the given nodes

$$\boldsymbol{r}(s) = [R(s, s_1), R(s, s_2), \text{L}, R(s, s_n)]^{\text{T}} \tag{2}$$

$\boldsymbol{A}$ and $\boldsymbol{B}$ are the temporary matrices

$$\begin{cases} \boldsymbol{M} = \boldsymbol{P}^T \boldsymbol{R}^{-1} \boldsymbol{P} \\ \boldsymbol{A} = \boldsymbol{M}^{-1} \boldsymbol{P}^T \boldsymbol{R}^{-1} \\ \boldsymbol{B} = \boldsymbol{R}^{-1}(\boldsymbol{I} - \boldsymbol{P}\boldsymbol{A}) \end{cases} \tag{3}$$

$\boldsymbol{P}$ is the $n \times m$ matrix that has basis function values at the given nodes.

$$\boldsymbol{P} = \begin{bmatrix} p_1(s_1) & p_2(s_1) & \text{L} & p_m(s_1) \\ p_1(s_2) & p_2(s_2) & \text{L} & p_m(s_2) \\ \text{M} & \text{M} & \text{O} & \text{M} \\ p_1(s_n) & p_2(s_n) & \text{L} & p_m(s_n) \end{bmatrix} \tag{4}$$

$\boldsymbol{R}$ is the $n \times n$ matrix of correlation between the given nodes

$$\boldsymbol{R} = \begin{bmatrix} 1 & R(s_1, s_2) & \text{L} & R(s_1, s_n) \\ R(s_2, s_1) & 1 & \text{L} & R(s_2, s_n) \\ \text{M} & \text{M} & \text{O} & \text{M} \\ R(s_n, z_1) & R(s_n, s_2) & \text{L} & 1 \end{bmatrix} \tag{5}$$

The correlation function $R(s_i, s_j)$ takes the form of Gaussian function in this work.

$$R(s_i, s_j) = \exp(-\frac{\omega r_{ij}^2}{d_m^2}) \tag{6}$$

where $r_{ij} = \left| s_i - s_j \right|$, d_m is the minimum distance between any two nodes on the local boundary, $\omega > 0$ is a correlation parameter and $\omega = 0.03 \sim 0.2$ is recommended [30].

$\boldsymbol{N}(s)$ has the following properties:

Kronecker delta property

$$N_I(s_J) = \delta_{IJ} \tag{7}$$

, consistency property

$$\sum_{i=1}^{n} N_i(s) s_i^j = s^j \quad (j = 0, 1, \text{L}, m-1) \tag{8}$$

and partition of unity property

$$Sum(\boldsymbol{N}(\text{s})) = \sum_{i=1}^{n} N_i(s) = 1 \tag{9}$$

The Kronecker delta property enables the boundary condition to be imposed directly and the results to be obtained directly, and the consistency property ensures high accuracy of the approximation.

3 Boundary node method for galvanic corrosion

3.1 Governing equations

The equation governing the potential distribution and the current flow in the electrolyte can be derived from charge conservation. The continuity equation requires that the current per unit volume, $\boldsymbol{J}$, relates to the charge, q, by

$$\nabla \boldsymbol{J} = \frac{\partial q}{\partial t} \tag{10}$$

Taking into account the relationship of electric field intensity, $\boldsymbol{E}$,

$$\boldsymbol{E} = -\nabla \phi \tag{11}$$

and Ohms law,

$$\boldsymbol{I} = \sigma \boldsymbol{E} \tag{12}$$

where σ is the conductivity of the electrolyte, the continuity equation transforms to

$$\nabla(\sigma \nabla \phi) = -\nabla(\frac{\partial q}{\partial t}) \tag{13}$$

Galvanic corrosion is a very slow process, thus we can make the following assumptions:
1. The electrolyte solution is well mixed that the conductivity is isotropic, σ is a constant.
2. The solution is electro-neutral, $\frac{\partial q}{\partial t} = 0$.

With the above assumptions, Eq. (13) can be simplified as,

$$\nabla^2 \phi = 0 \tag{14}$$

Therefore, for a uniform, isotropic electrolyte, the potential obeys the Laplace equation.

3.2 Boundary condition

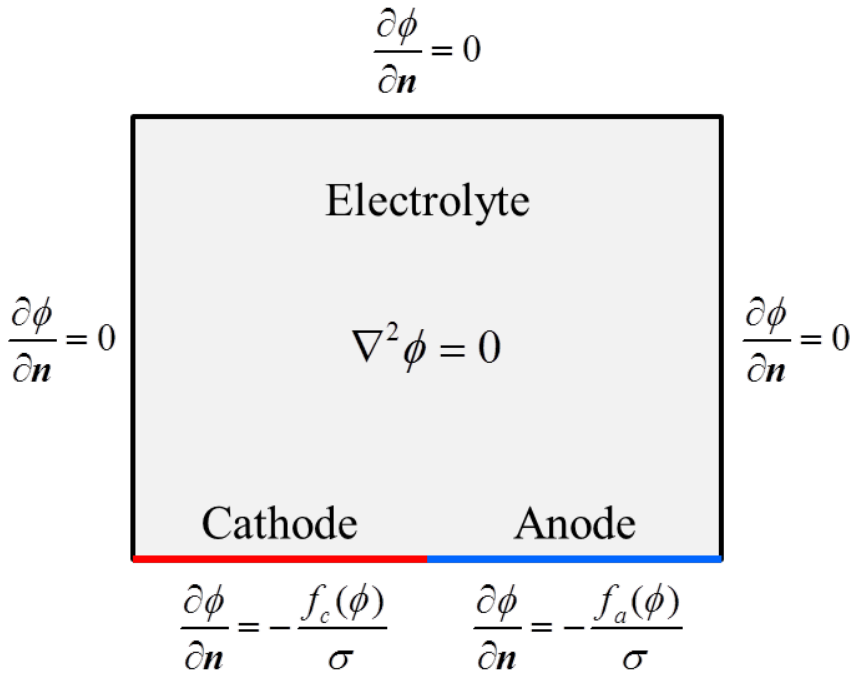

Figure 1. Schematic of the mathematical model of galvanic corrosion

Eq. (14) can be solved with the boundary conditions shown schematically in Figure 1. The boundary conditions at the anode and the cathode surfaces are vital to predict the corrosion rates. The boundary condition applied at the anode surface Γ_a is:

$$\frac{\partial \phi}{\partial \boldsymbol{n}} = -\frac{j}{\sigma} = -\frac{f_a(\phi)}{\sigma} \tag{15}$$

where σ is the electrical conductivity of the electrolyte solution and $f_a(\phi)$ is the current density determined by anodic species. $f_a(\phi)$ is a piecewise linear interpolation function which is obtained from the polarization curve of the anodic species. Thus, we use a piecewise linear interpolation approach to handle non-linear boundary conditions.

Similarly, the boundary condition applied at the cathode surface Γ_c is

$$\frac{\partial \phi}{\partial \boldsymbol{n}} = -\frac{f_c(\phi)}{\sigma} \tag{16}$$

The boundary condition applied at the insulation surface and the electrolyte-air interface Γ_{ins} is

$$\frac{\partial \phi}{\partial \boldsymbol{n}} = -\frac{j}{\sigma} = 0 \tag{17}$$

3.3 BNM formulation

In summary, the governing equation and the boundary conditions are

$$\begin{cases} \Delta\phi = \dfrac{\partial^2 \phi}{\partial x^2} + \dfrac{\partial^2 \phi}{\partial y^2} = 0 & \text{in } \Omega \\ \dfrac{\partial \phi}{\partial \boldsymbol{n}} = -\dfrac{f_a(\phi)}{\sigma} & \text{on } \Gamma_a \\ \dfrac{\partial \phi}{\partial \boldsymbol{n}} = -\dfrac{f_c(\phi)}{\sigma} & \text{on } \Gamma_c \\ \dfrac{\partial \phi}{\partial \boldsymbol{n}} = 0 & \text{on } \Gamma_{ins} \end{cases} \tag{18}$$

where ϕ is the potential, $j = -\sigma \dfrac{\partial u}{\partial \boldsymbol{n}}$ is the current density along the normal of the boundary, the whole boundary is $\Gamma = \partial\Omega = \Gamma_a + \Gamma_c + \Gamma_{ins}$. The integral representation of the solution for Eq. (18) is

$$c(\boldsymbol{\xi})\phi(\boldsymbol{\xi}) + \int_\Gamma \frac{\partial \phi^*(\boldsymbol{x}\text{-}\boldsymbol{\xi})}{\partial \boldsymbol{n}} \phi(\boldsymbol{x}) \mathrm{d}\Gamma = \frac{-1}{\sigma} \int_\Gamma \phi^*(\boldsymbol{x}\text{-}\boldsymbol{\xi}) j(\boldsymbol{x}) \mathrm{d}\Gamma \tag{19}$$

where $\boldsymbol{\xi}$ denotes the given source point on the boundary,

$\boldsymbol{x}$ denotes a filed point on the boundary,

$\phi^*(\boldsymbol{x}\text{-}\boldsymbol{\xi}) = -\dfrac{1}{2\pi} \ln |\boldsymbol{x} - \boldsymbol{\xi}|$ is the fundamental solution of Laplace's equation,

$\dfrac{\partial \phi^*}{\partial \boldsymbol{n}}$ is the normal derivative of ϕ^* on the boundary,

$c(\boldsymbol{\xi})$ is a coefficient related to the boundary smoothness.

The boundary Γ is divided into background cells Γ_i $(i = 1, 2, 3, \mathrm{L}, m)$ for numerical integration, and the discrete form of Eq. (19) is

$$c(\boldsymbol{\xi})u(\boldsymbol{\xi})+\sum_{i=1}^{m}\int_{\Gamma_i}\frac{\partial\phi^*(\boldsymbol{x}-\boldsymbol{\xi})}{\partial\boldsymbol{n}}\phi(\boldsymbol{x})\mathrm{d}\Gamma=\frac{-1}{\sigma}\sum_{i=1}^{m}\int_{\Gamma_i}\phi^*(\boldsymbol{x}-\boldsymbol{\xi})\,j(\boldsymbol{x})\mathrm{d}\Gamma \tag{20}$$

$u(\boldsymbol{x})$ and $q(\boldsymbol{x})$ are approximated by MKI.

$$\begin{cases} u=\boldsymbol{N}(s)\boldsymbol{\Phi}=\sum_{k=1}^{n}\varphi_k(s)\phi_k \\ j=\boldsymbol{N}(s)\boldsymbol{Q}=\sum_{k=1}^{n}\varphi_k(s)\,j_k \end{cases} \tag{21}$$

To track the moving boundary, $\boldsymbol{x}$ is also approximated by MKI.

$$\boldsymbol{x}=\boldsymbol{N}(s)\boldsymbol{X}=\sum_{k=1}^{n}\varphi_k(s)\boldsymbol{x}_k \tag{22}$$

Substituting Eq. (21) into Eq. (20) yields

$$c(\boldsymbol{\xi})\phi(\boldsymbol{\xi})+\sum_{i=1}^{m}\int_{\Gamma_i}\frac{\partial\phi^*(\boldsymbol{x}-\boldsymbol{\xi})}{\partial\boldsymbol{n}}\boldsymbol{N}(s)\boldsymbol{\Phi}\mathrm{d}\Gamma=\frac{-1}{\sigma}\sum_{i=1}^{m}\int_{\Gamma_i}\phi^*(\boldsymbol{x}-\boldsymbol{\xi})\boldsymbol{N}(s)\boldsymbol{J}\mathrm{d}\Gamma \tag{23}$$

Employing numerical methods for the integrals in Eq. (23), at every nodes, we can obtain the linear algebraic equations.

$$\boldsymbol{C\Phi}+\hat{\boldsymbol{H}}\boldsymbol{\Phi}=\boldsymbol{GJ} \tag{24}$$

where

$$\boldsymbol{C}=diag(c(\boldsymbol{\xi}_1),c(\boldsymbol{\xi}_2),\mathrm{L}\ ,c(\boldsymbol{\xi}_n)) \tag{25}$$

$$\hat{\boldsymbol{H}}_i=\sum_{k=1}^{m}\int_{\Gamma_k}\frac{\partial\phi^*(\boldsymbol{x}-\boldsymbol{\xi}_i)}{\partial\boldsymbol{n}}\boldsymbol{N}(s)\mathrm{d}\Gamma \tag{26}$$

$$\boldsymbol{G}_i=\frac{-1}{\sigma}\sum_{k=1}^{m}\int_{\Gamma_k}\phi^*(\boldsymbol{x}-\boldsymbol{\xi}_i)\boldsymbol{N}(s)\mathrm{d}\Gamma \tag{27}$$

Let

$$\boldsymbol{H}=\boldsymbol{C}+\hat{\boldsymbol{H}} \tag{28}$$

Eq. (24) can then be rewritten as

$$\boldsymbol{H\Phi}=\boldsymbol{GQ} \tag{29}$$

Normally, we do not directly compute $\boldsymbol{C}$, because the diagonal elements of $\boldsymbol{H}$ can be computed by constant potential method.

$$H_{ii}=-\sum_{k=1,\mathrm{k}\neq i}^{n}H_{ik} \tag{30}$$

Finally, we can solve Eq. (29) with the boundary conditions in Eq. (18) and obtain the nodal values of potential and current density on the boundary.

4 Case study

The MKIBNM method, for the first time, is applied to investigate the corrosion behavior of AE44 (Mg, Anode)–mild steel (Cathode) couple which is exposed to 1.6 wt.% NaCl (electrolyte) solution. The numerical model is shown in Figure 2. The basis function of MKI is $\boldsymbol{p}(s)=[1,s,s^2]$ and the correlation function is Gaussian function with $\omega=0.1$. The polarization data in Figure 1 from reference [22] are used as the boundary condition for the anode and the cathode surfaces. The conductivity of the electrolyte σ is 2.5 S/m.

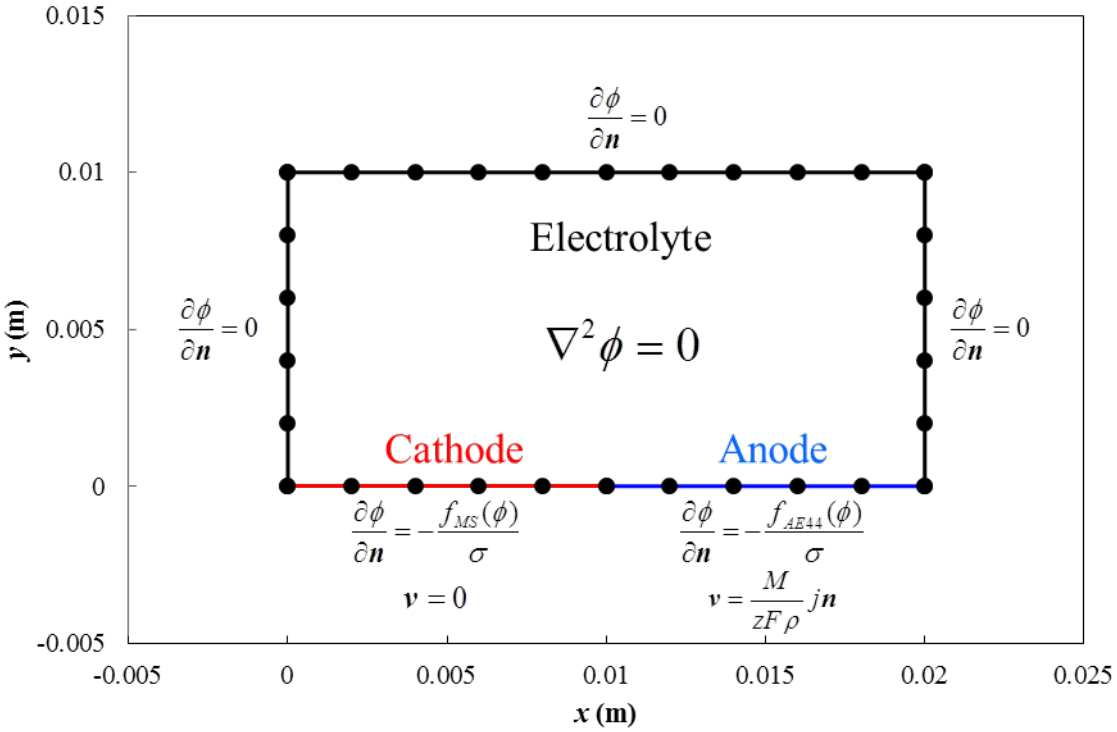

Figure 2. Numerical model of BNM for the corrosion of the galvanic couple.

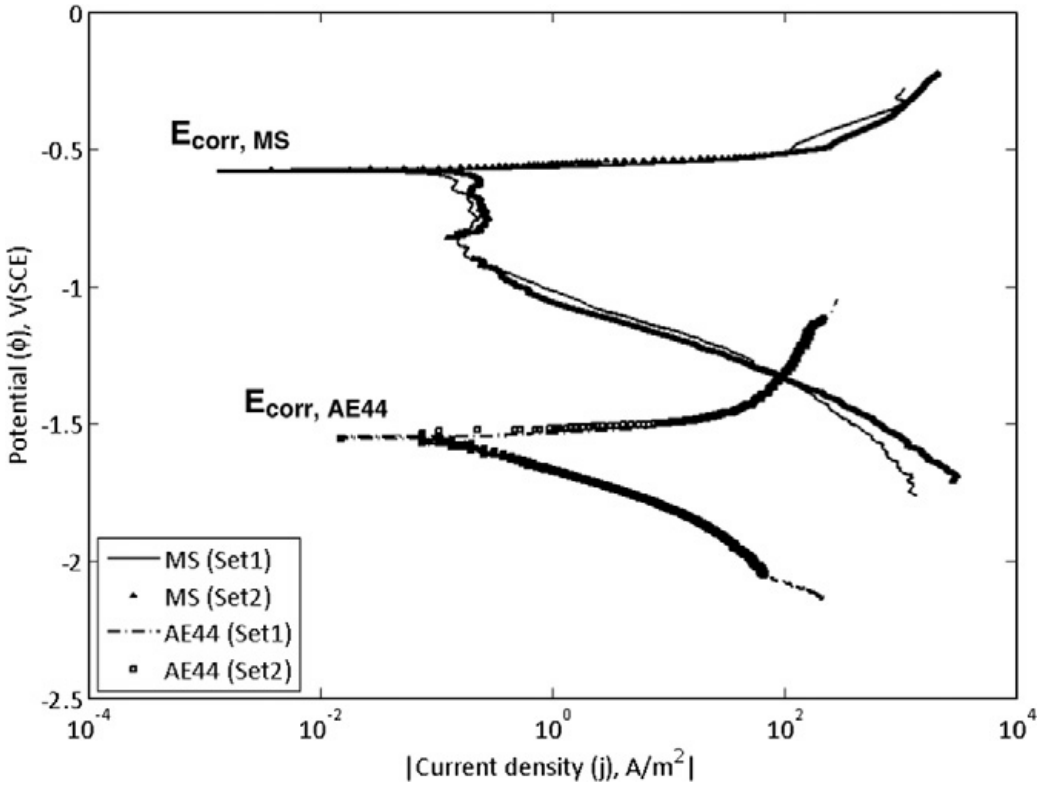

Figure 3. Polarization behaviour of mild steel and AE44 [22].

The initial current density along the anode and the cathode surfaces is plotted in Figure 4. It can be seen that the initial peak current density at the anodic region predicted by the model is 84.8 A/m^2 and the current density gradually decreases to around 29.1 A/m^2 away from the junction. The initial current density obtained from the experiment [21] [22] is also plotted in Figure 4 for comparing. The peak anodic current density at the junction of the couple obtained from the experiments is about 81.6 A/m^2. Thus, the numerical estimate of the peak anodic

current density is within 4% of that obtained from the experiment. The current density profile over the anodic and the cathodic regions obtained from MKIBNM agrees well with the profile obtained from the experiments.

The corrosion rate can be estimated from the anodic current density using Eq.(31).

$$C_R = \frac{M}{zF\rho} j \tag{31}$$

Where F is the Faraday constant, 96485.34 C/mol,

M is the atomic mass, 26.82 g/mol,

z is the electron number, 2,

ρ is the densityfor the anode AE44, 1820 kg/m^3,

C_R is corrosion rate,

j is the current density.

In the numerical model, the position of the moving anode surface can be evaluated from the transient current density.

$$(dx, dy) = \mathbf{v}\delta t = \frac{M}{zF\rho} j\mathbf{n}\delta t \tag{32}$$

The profile of the anode surface for AE44–mild steel couple obtained from the numerical model with time step $\delta t = 1\text{h} = 3600\text{s}$ after 3 days of constant exposure to the electrolyte solution is shown in Figure 5. It can be seen that a 1.8 mm deep pit at the AE44 side of the galvanic couple is predicted by the numerical model. The surface profile predicted using the numerical model can also be validated using the immersion experiment [21] [22]. The surface profile of AE44–mild steel couple after 3 days of immersion in 1.6 wt.% NaCl solution is shown in Figure 5. A 2.0 mm deep pit is formed at the junction. Thus, the numerical prediction of the pit depth is within 10% of that obtained from the immersion experiment for AE44 – mild steel couple.

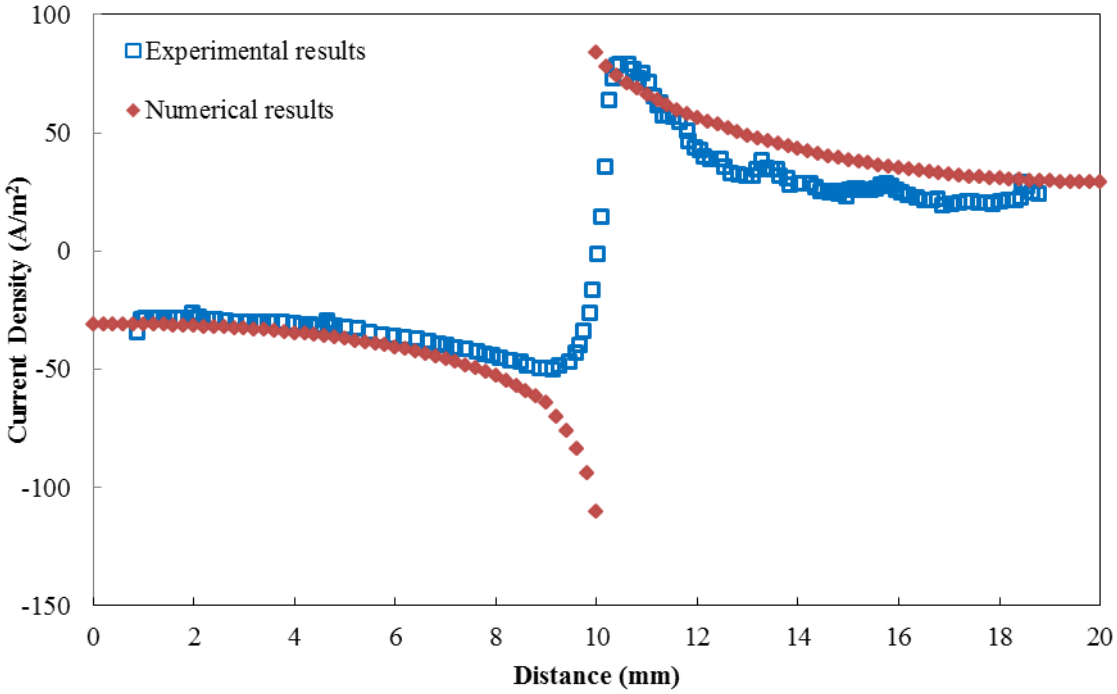

Figure 4 The initial spatial current density variation predicted using the numerical model and obtained from experiments

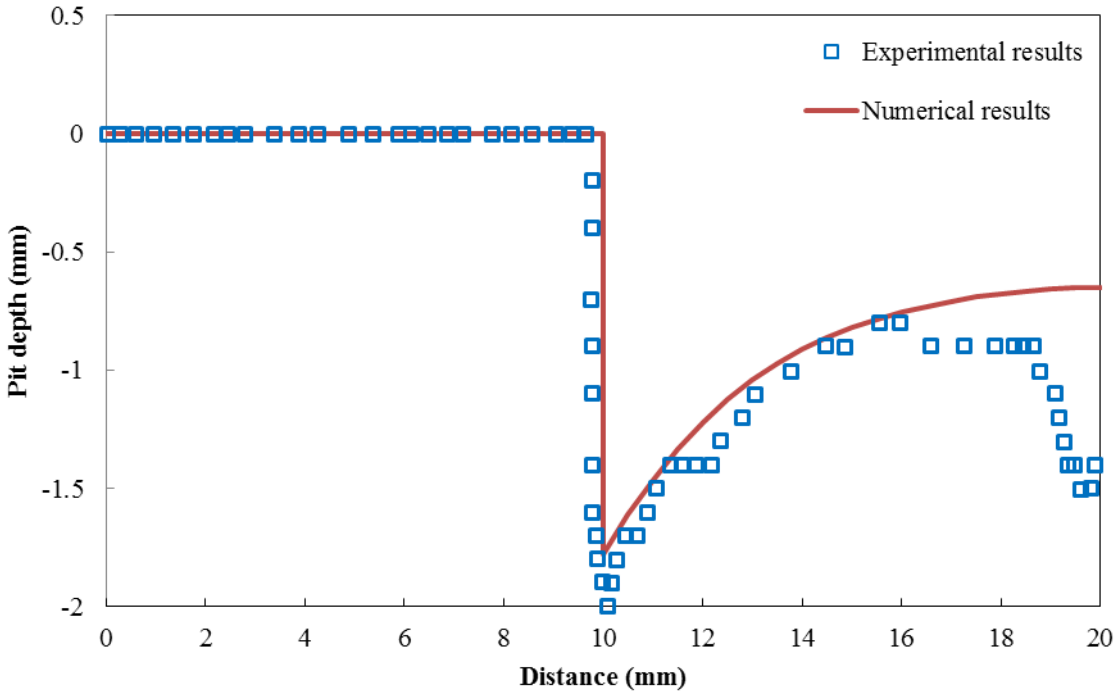

Figure 5 The surface profile predicted using the numerical model and obtained from the immersion experiment

5 Conclusions

1. A MKI-based BNM method developed in this work is capable of tracking a moving boundary during galvanic corrosion and can handle non-linear boundary conditions.
2. The numerical estimate of the peak anodic current density is within 4% of that obtained from the experiment. The numerical prediction of the pit depth is within 10% of that obtained from the experiment.
3. The MKI-based BNM is an effective and flexible method to simulate the process of galvanic corrosions.

Acknowledgement

This research was sponsored by Key Projects in the National Science & Technology Pillar Program during the Thirteenth Five-year Plan Period of China (No. 2016ZX05057012).

References

[1] Liu, G. R. and Liu, M. B. (2003) *Smoothed Particle Hydrodynamics — A Meshfree Particle Method*, World Scientific, Singapore.
[2] Cui, X. Y., Feng, H., Li, G. Y. and Feng, S. Z. (2015) A cell-based smoothed radial point interpolation method (CS-RPIM) for three-dimensional solids, *Engineering Analysis with Boundary Elements* **50**, 474-485
[3] Zheng, B. J. and Dai, B. D. (2011) A meshless local moving Kriging method for two-dimensional solids, *Applied Mathematics and Computation* **218**, 563-573
[4] Peng, M. J., Liu, P. and Cheng, Y. M. (2009) The Complex Variable Element-Free Galerkin (Cvefg) Method for Two-Dimensional Elasticity Problems, *International Journal of Applied Mechanics* **1**, 367-385
[5] Cheng, Y. M., Li, R. X. and Peng, M. J. (2012) Complex variable element-free Galerkin method for viscoelasticity problems, *Chinese Physics B* **21**, 090205
[6] Deng, Y. J., Liu, C., Peng, M. J. and Cheng, .Y. M. (2015) The Interpolating Complex Variable Element-Free Galerkin Method for Temperature Field Problems, International Journal of Applied Mechanics 7, 1550017
[7] Mukherjee, Y. X. and Mukherjee, S. (1997) The boundary node method for potential problems, *International Journal for Numerical Methods in Engineering* **40**, 797-815

[8] Chati, M. K., Mukherjee, S. and Mukherjee, Y. X. (1999) The boundary node method for three-dimensional linear elasticity, *International Journal for Numerical Methods in Engineering* **46**, 1163-1184
[9] Kothnur, V. S., Mukherjee, S. and Mukherjee, Y. X. (1999) Two-dimensional linear elasticity by the boundary node method, *International Journal of Solids and Structures* **36**, 1129-1147
[10] Chati, M. K. and Mukherjee, S. (2000) The boundary node method for three-dimensional problems in potential theory, *International Journal for Numerical Methods in Engineering* **47**, 1523-1547
[11] Lancaster, P. and Salkauskas, K. (1981) Surfaces generated by moving least squares methods, *Mathematics of Computation* **37**, 141-158
[12] Zhu, T., Zhang, J. and Atluri, S. N. (1998) A meshless local boundary integral equation (LBIE) method for solving nonlinear problems, *Computational Mechanics* **22**, 174-186
[13] Zhu, T., Zhang, J. D. and Atluri, S. N. (1998) A local boundary integral equation (LBIE) method in computational mechanics, and a meshless discretization approach, *Computational Mechanics* **21**, 223-235
[14] Liew, K. M., Cheng, Y. M. and Kitipornchai, S. (2005) Boundary element-free method (BEFM) for two-dimensional elastodynamic analysis using Laplace transform, *International Journal for Numerical Methods in Engineering* **64**, 1610-1627
[15] Liew, K. M., Cheng, Y. M. and Kitipornchai, S. (2006) Boundary element-free method (BEFM) and its application to two-dimensional elasticity problems, *International Journal for Numerical Methods in Engineering* **65**, 1310-1332
[16] Liew, K. M. and Cheng, Y. M. (2009) Complex variable boundary element-free method for two-dimensional elastodynamic problems, *Computer Methods in Applied Mechanics and Engineering* **198**, 3925-3933
[17] Ren, H. P., Cheng, Y. M. and Zhang, W. (2009) An improved boundary element-free method (IBEFM) for two-dimensional potential problems, *Chinese Physics B* **18**, 4065-4073
[18] Ren, H. P., Cheng, Y. M. and Zhang, W. (2010) An interpolating boundary element-free method (IBEFM) for elasticity problems, *Science China-Physics Mechanics & Astronomy* **53**, 758-766
[19] Li, X. G., Dai, B. D. and Wang, L. H. (2010) A moving Kriging interpolation-based boundary node method for two-dimensional potential problems, *Chinese Physics B* **19**, 120202
[20] Gu, L. (2003) Moving Kriging interpolation and element-free Galerkin method, *International Journal for Numerical Methods in Engineering* **56**, 1-11
[21] Deshpande, K. B. (2010). Experimental investigation of galvanic corrosion: comparison between svet and immersion techniques. *Corrosion Science*, **52**(9), 2819-2826.
[22] Deshpande, K. B. (2010). Validated numerical modelling of galvanic corrosion for couples: magnesium alloy (ae44)–mild steel and ae44–aluminium alloy (aa6063) in brine solution. *Corrosion Science*, **52**(10), 3514-3522.
[23] Trinh, D., Dauphin, D. P., Mengesha, T. U., Kish, J. R., & Mauzeroll, J. (2012). Influence of edge effects on local corrosion rate of magnesium alloy/mild steel galvanic couple. *Analytical Chemistry*, **84**(22), 9899-906.
[24] Jia, J. X., Song, G., and Atrens, A. (2007). Experimental measurement and computer simulation of galvanic corrosion of magnesium coupled to steel. *Advanced Engineering Materials*, **9**(1-2), 65-74.
[25] Murer, N., Oltra, R., Vuillemin, B., & Néel, O. (2010). Numerical modelling of the galvanic coupling in aluminium alloys: a discussion on the application of local probe techniques. *Corrosion Science*, **52**(1), 130-139.